Journal of Marine Research, 59, 991–1020, 2001

Effects of macrofauna on acoustic backscatter from the seabed: Field manipulations in West Sound, Orcas Island, Washington, U.S.A.

by Robert F. L. Self[1], Patrick A'Hearn[1,2], Peter A. Jumars[3], Darrell R. Jackson[4], Michael D. Richardson[5] and Kevin B. Briggs[5]

ABSTRACT

Previous observations with a bottom-mounted, radially scanning sonar (BAMS) at 40 kHz suggested that macrofaunal activities influence low-angle, acoustic backscatter from seafloor sediments. In order to test that possibility experimentally, we measured and modeled time series of backscatter strength at both 40 and 300 kHz prior to manipulation and then introduced several macrofaunal species at known abundances to randomly selected locations within the ensonified area. We worked in West Sound, Orcas Island, Washington, at a water depth of 20.4 m and for the more frequently recorded 40-kHz series extracted effects by the time-series method known as "intervention analysis," wherein the intervention was the experimental alteration. We observed increased backscatter from patches of the small protobranch bivalve *Acila castrensis,* and of the cockle *Clinocardium nuttali,* from bait used as chum for fishes and crabs, and from tethered crabs (*Cancer magister*); other treatments showed no significant change. All of the effective treatments involved increased backscatter at 300 kHz from animals that have obvious hard parts or air bladders. Power calculations for intervention analysis and geoacoustic modeling suggest that failure of other treatments to show significant effects on backscatter strength stems from the small size of the organisms and structures used relative to the 40-kHz wavelength (3.7 cm) and to low sound-speed contrasts between surficial sediments at this site and overlying water (at both frequencies), producing low backscatter levels from both volume heterogeneity and surface microtopography. This experiment demonstrates, however, that low-angle acoustic backscatter can be used to observe at least some populations of benthic animals over a large area (ca. 8000 m^2) and that intervention analysis can be a useful tool where logistics permit repeated observation but few or no spatial replicates—frequently the case in ecological manipulations.

1. School of Oceanography, Box 357940, University of Washington, Seattle, Washington, 98195-7940, U.S.A.

2. Present address: Joint Institute for the Study of the Atmosphere and Ocean, Box 357941, University of Washington, Seattle, Washington, 98195-7941, U.S.A.

3. Darling Marine Center, University of Maine, 193 Clark's Cove Road, Walpole, Maine, 04573-3307, U.S.A. ***email: jumars@maine.edu*** (corresponding author).

4. Applied Physics Laboratory, Box 355640, University of Washington, Seattle, Washington, 98195-5640, U.S.A.

5. Naval Research Laboratory, Seafloor Sciences Branch, Stennis Space Center, Mississippi, 39529-5004, U.S.A.

1. Introduction

Recent studies have found putatively biological or biogenic signals in low-angle acoustic backscatter data from subtidal regions (Jumars *et al.,* 1996; Briggs and Richardson, 1997). Backscattered acoustic signals are attractive because unlike any method in current use for study of benthos, they afford rapid, wide-area coverage of the seabed. In order to test the hypothesis that this technique can observe benthic animals and (or) their effects, we conducted a "ground truth" experiment. We deployed a modified version of the tripod-mounted 40-kHz acoustic transducer system developed by Dworski and Jackson (1994)—with the addition of a new, 300-kHz transducer—in 20.4 m of water in West Sound, Orcas Island, Washington, USA. SCUBA divers placed a variety of organisms on the bottom for acoustic observation, including burrowing shrimp (*Neotrypaea californiensis* and *Upogebia pugettensis*), burrowing urchins (*Brisaster latifrons*), burrowing sea cucumbers (*Molpadia intermedia*), crabs (*Cancer magister*), large cockles (*Clinocardium nuttallii*) and small bivalves (*Acila castrensis*). In addition, we placed bait on the bottom to attract fishes and crabs, and fashioned mimics of pits, mounds and vertical burrows. We monitored these treatments for 6 to 17 d for changes in acoustic properties. All treatments involving target animals with hard parts or air bladders showed significant backscatter, except for the urchin treatment. Although no other treatments showed significant effects, this method of quickly scanning large areas shows promise for detecting and monitoring some kinds of benthic animals and their activities. Furthermore, the statistical technique of intervention analysis allowed a clear statement of the threshold backscatter strength defining a treatment effect and shows great promise for broader application to manipulations wherein logistics limit the number of replicates but make time-series observations feasible. Some preliminary data from our manipulations, along with analyses of backscatter from man-made objects placed on the seafloor have been published (Williams, 2001).

2. Methods

a. Site

The experimental site is centered on 48° 37.32′N, 122° 58.36′W in West Sound, Orcas Island, Washington, USA (Fig. 1). Criteria for its selection included high horizontal uniformity of the seabed, low bottom slope and low abundances of large, resident megafauna that might be confused with experimental treatments. Timing and resources did not allow pre-experiment survey of acoustic properties as part of site selection. The site is a sheltered area with a level mud bottom and depth of 20.4 m. Maximal tidal range during the experiment was 2.75 m.

b. Sonar and ancillary data

To collect the primary acoustic data in this study, two sonar transducers, operating at 40 and 300 kHz, respectively, were mounted on a rotating head atop a bottom-landing tripod,

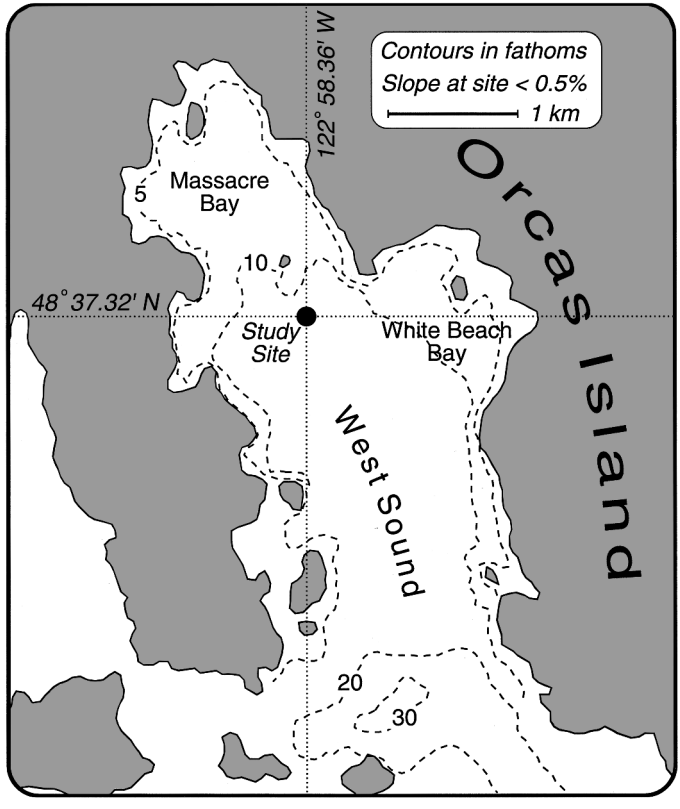

Figure 1. Site map, West Sound, Orcas Island, Washington, U.S.A. Modified from NOAA Chart.

5.4 and 5.2 m above the bottom, respectively (cf. Fig. 1 of Williams, 2001). The 300-kHz transducer has a 1° horizontal full-width half-maximum in beam geometry and a 30° vertical spread. The 40-kHz transducer has a 5° horizontal full-width half maximum, and a 14.5° vertical spread. Both were centered 12° below horizontal. Transmitted pulses were 2-ms long FM sweeps from 290 to 310 kHz for the 300-kHz system and 39 to 41 kHz for the 40-kHz system. The 300-kHz transducer was rotated in 1° steps every 5 s, completing a 360° scan in 30 min. The 40-kHz transducer was rotated in 5° steps every 5 s, completing a 360° scan in 6 min. Received signals were recorded as a complex time series of amplitude and phase information at 20 kHz for 120 ms (300 kHz) and 2 kHz for 108 ms (40 kHz), providing a maximal one-way path length of ~85 m. Complete 300-kHz scans were taken twice daily at 2200 and 0300 hours, this timing selected to give two scans of the acoustic marker spheres for precise location of treatments. Ten, evenly spaced, 40-kHz scans were taken daily beginning at 0140 hours on July 29, 1995 and ending at 2300 hours on September 25, 1995. The number of scans was limited by power and data-storage capacity on the tripod.

Computer processing for backscatter strength took several steps. First the complex (phase and amplitude) time signal was match filtered (Skolnik, 1980) to enhance spatial resolution. The match-filtered time series from each ping was binned into segments corresponding to 0.075 m (300 kHz) or 0.5 m (40 kHz) radial increments of the seafloor. The time-series amplitude was then squared to get received level in decibels, corrected for transmission loss, and adjusted for angular effects with a Lambertian $[\sin(\text{grazing angle})]^2$ term (Urick, 1983). This procedure provided a backscatter level for each pixel, assuming that the bottom is a Lambertian reflector. Departures from Lambert's law would introduce range (grazing angle) dependence, but it appears to apply reasonably well (Williams, 2001), and where departure might present serious problems (spatial autocorrelation) range dependence was removed.

A Sea-Bird CTD (Seacat 19) was mounted on the tripod to record temperature, salinity and pressure every 2 min. CTD profiles were measured approximately weekly with a custom Sea-Bird CTD, 50 m SSE of the tripod.

c. Experimental treatments

Each treatment had one replicate located in each of three 74°-wide sectors (Fig. 2). The remaining 138° sector observed by BAMS was used for other experiments by other groups of investigators (e.g., Williams, 2001). Each replicate was randomly assigned a radial position between 15 and 30 m from the tower (~10–20° grazing angle) and an azimuthal position between 0 and 74° within its sector. Using a hand-held compass and several reference floats, on the day prior to the manipulation we dropped an acoustic marker from a boat at each of the assigned locations. These markers consisted of a 0.2-m (diam), liquid-filled acoustic reflector and lead weight resting on the bottom, and a surface float, all attached to a nylon line. The two 300-kHz scans the following night showed 3 locations of very high backscatter strength. The following day, divers followed the lines and conducted bottom manipulations at the locations of the markers. When the divers returned to the surface, we retrieved the acoustic markers and placed them at the locations of the next day's experiments. Revisiting experimental treatments after emplacement was impractical; almost any sort of marking device could have affected acoustic properties, and the water was generally too turbid for divers to see features on the bottom directly.

We deployed ten experimental treatments, generally in triplicate. Under each description, quantities refer to each replicate. The first term before the colon in each case is the informal shorthand that we applied to designate treatments and discuss results.

(1) *Acila:* We "sprinkled" about 4400 ± 600 (mean ± SD) protobranch bivalves, *Acila castrensis,* on a 1-m^2 area of the bottom, about 1.45 liters of clams per replicate. Mean largest measurement (anterior-posterior length) was 1.0 cm. *A. castrensis* is found at lower population density than this treatment at the entrance to West Sound (~2.8 km away) and occurs even more sparsely at the study site. A few of their shells were observed in the X-radiographs from the experimental site. Animals for the experiment were dredged from

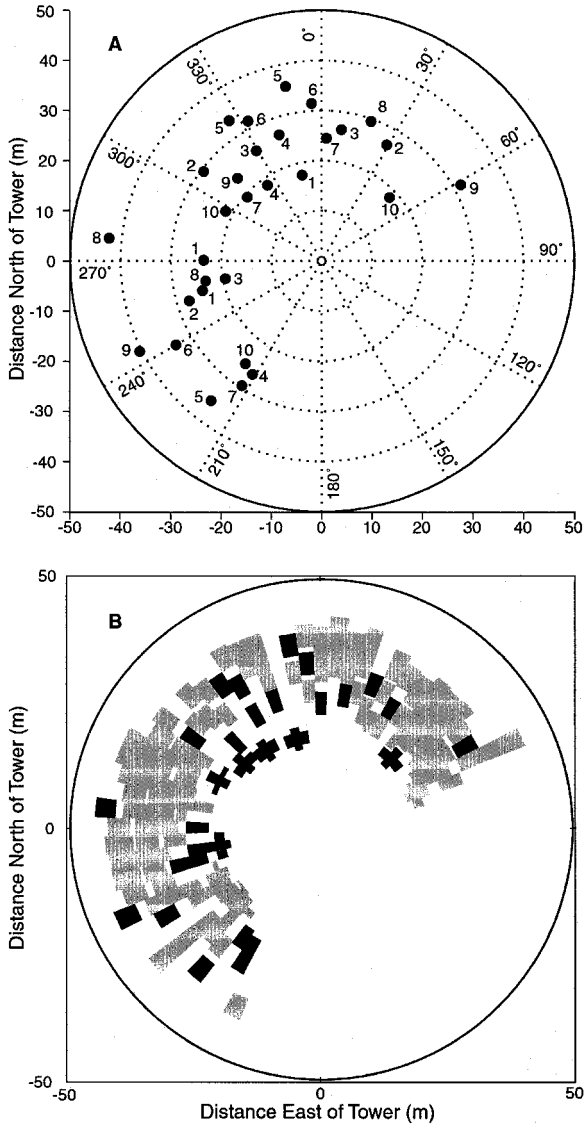

Figure 2. (A) Scan geometry in both circular and Euclidean coordinates. The open area in the southeast sector of the scan circle was devoted to experiments with buried and proud (unburied), mine-like objects and has been treated elsewhere (Williams, 2001). Filled circles are centered on acoustically-determined (300 kHz) reflector locations, adjacent numbers indicating the treatments applied (1, *Acila;* 2, mounds and pits; 3, shrimp; 4, diver control; 5, urchins; 6, bait; 7, cockles; 8, burrows; 9, *Molpadia;* 10, tethered crab). (B) Planar plot of the ensonified area at 40 kHz resolution. Pixels are 5° in azimuthal and 0.5 m in radial extent. Black pixels denote treatment locations; grey areas comprise 963 untreated control pixels from which empirical frequency distributions were generated.

Lopez Sound, Lopez Island, Washington, at 15 m depth. Densities produced by our procedure are greater than natural levels even there by a factor of 5–10.

(2) Mounds and pits: We produced vertical relief in clusters of paired mounds and pits. A 15-cm diam core tube was pushed into the bottom to a depth of approximately 20 cm, leaving a cylindrical hole. The core material was then placed on the bottom adjacent to the hole. For each replicate, four such holes and mounds were formed within a 1-m^2 area.

(3) Shrimp: We placed 50 *Neotrypaea californiensis* and 5 *Upogebia pugettensis* in a bottomless cage on the seafloor. Overall length (tip of rostrum to tip of tail) ranged from 6.5–8.5 cm for *Neotrypaea* and from 6.8–9.2 cm for *Upogebia.* The cage had a 50 × 80 cm opening to the bottom and was left in place for approximately 1 h while the shrimp burrowed; then the cage was removed. It kept the shrimp confined to the experimental location and possibly reduced predation while they burrowed. Diver observations showed that most shrimp did indeed burrow within the hour allotted; potential predators, crabs of the genus *Cancer,* were often found clinging to the cage when it was removed. Shrimp were collected from the intertidal of False Bay, San Juan Island, Washington.

(4) Diver control: As a control for diver-generated disturbance, divers descended to the acoustic markers, landed on the bottom as they would to put in an experimental treatment, then returned to the surface.

(5) Urchins: We placed 24 (22 for one replicate) burrowing heart urchins, *Brisaster latifrons,* by hand slightly below the sediment surface in a 1-m^2 area. They had mean dimensions 6.3 × 5.7 × 3.5 cm. Animals were collected with van Veen grabs in Puget Sound at the 200-m site described by Nichols (1975).

(6) Bait: We hose clamped a 7.5 cm diameter × 10 cm cylindrical can of Western Family™ "fish and chicken flavor" cat food to one end of a 1-m length of 0.5 in (1.3 cm) diam steel rebar. Divers then perforated the cans and pushed the unit into the sediment so that only the short length of rebar with the can attached projected above the seafloor.

(7) Cockles: We placed 10 *Clinocardium nuttallii,* with mean dimensions 6.8 cm (longest anterior-posterior length) × 6.7 cm (longest dorsoventral length, from umbo) × 4.9 cm (maximal lateral width) just below the sediment surface. Animals were collected from the intertidal of False Bay, San Juan Island, Washington.

(8) Burrows: Divers pushed pointed, 2.3-cm diameter wooden dowels vertically into the sediment, leaving 30 simulated burrows approximately 20 cm deep in a 1-m^2 area.

(9) *Molpadia:* We placed 38 burrowing sea cucumbers, *Molpadia intermedia,* just below the sediment surface. Mean dimensions were 10.9 cm long × 2.4 cm diameter. Animals were collected with a van Veen grab in Puget Sound at the 200-m site described by Nichols (1975).

(10) Tethered crab: We "leashed" individual Dungeness crab, *Cancer magister,* with a 1-m long, braided stainless steel wire to a T-handled, 1-m length of ½-in (1.3 cm) rebar pushed into the sediment. Crabs were 15.0, 16.0 and 16.5 cm wide across the carapace. These animals were collected by divers or intertidally.

d. The 300 kHz analysis

Each replicate's position was determined from the strongest-reflecting pixel in a computer-screen representation of the bottom—assumed to be produced by its acoustic marker (Fig. 2A). Since actual locations and dimensions of the treatments did not correspond exactly with the markers, we examined all pixels whose centers fell within 2 m of the marker pixel's center. Individual pixel area varies with distance from the tower.

Because backscatter measurements were made sequentially within a contiguous region, the assumption of statistical independence among pixels adjacent in time or space is dubious. We tested for background temporal autocorrelation in nontreatment pixels with Pearson's product-moment correlation coefficient (Sokal and Rohlf, 1995) and, when encountering small sample sizes, confirmed trends with its nonparametric equivalent, Kendall's τ (Press *et al.,* 1988). Moran's I (Cliff and Ord, 1973), the spatial equivalent of the product-moment correlation coefficient, estimated spatial similarity between nontreatment pixels with intersample distances (pixel center to pixel center) 0.075–100 m apart. The size of the data sets (239,760 pixels per each of 62 300-kHz scans; 7200 pixels per each of 585 40 kHz scans) and limited computer resources forced us to rely on sampled randomization tests (Sokal and Rohlf, 1995) to estimate spatial autocorrelation. We selected 1,000 pixels at random to generate temporal and spatial correlograms. We likewise determined confidence limits for Moran's I coefficients from the same pixel set selected for the correlograms. Random normal deviates with the same mean and variance as the original 1000 values in the randomization test were assigned to the same pixel set and the coefficients recalculated. Because we found significant spatial autocorrelation, we detrended the data by subtracting the mean backscatter strength at the pixel's radial range (at the time of that particular sonar scan) from each pixel's value (Jumars *et al.,* 1996). The residual backscatter strengths were used to assess changes in backscatter strength due to our manipulations.

We found no temporal autocorrelation after detrending the sparse 300-kHz backscatter strength series (see Results and discussion). Therefore, at each post-treatment time point, we assigned each pixel in the treatment area a probability level based on the likelihood of its backscatter value appearing in the pre-treatment distribution. The pre-treatment distribution consisted of all backscatter values measured at that pixel location before emplacement of the experiment. Values more extreme than any in this distribution were given a conservative probability level of $1/(n + 1)$. The result was a time series of probability level for each pixel in a treatment area.

The final product was the overall significance for each pixel determined by combining the probabilities in its post-treatment time series by Fisher's method (Sokal and Rohlf, 1995). Assuming a chi-squared distribution with $2k$ degrees of freedom (k = number of measurements in the pre-treatment time series), we calculated the overall probability that the individual, post-treatment probabilities could have co-occurred by chance. Thus, individual or repeated, high or low backscatter-strength measurements during the treatment phase contributed to lower the chi-squared probability level.

Treatment areas, even as expanded by the 2-m search radius, were only a small proportion of the area ensonified by BAMS. By applying the same analytic protocol to randomly selected but untreated areas of the seafloor, we generated empirical distributions of the test statistics to serve as a further check on the validity of our analysis.

We analyzed four treatments for the high-backscatter tail: *Acila,* cockle, bait, and tethered crab. Bivalves and tethered crabs were hypothesized to increase backscatter strength from their calcareous shells and carapaces, respectively. We expected bait to attract fishes, crabs and other scavengers that would increase backscatter strength. We analyzed other treatments two tailed. Although volume heterogeneity (small-scale variations in sound speed) created by those treatments probably would raise backscatter intensity, we could imagine the possibility that unlike hard reflectors or swim bladders, the other features we produced could systematically or at least stochastically reflect or duct sound away from a return path. Therefore, we took the more conservative approach of analyzing significance for the remaining treatments two tailed.

e. The 40-kHz analysis

Detrending the data by subtracting the mean backscatter strength at the pixel's radial range from each pixel's value did not produce temporally uncorrelated residuals. Persistent time dependency required an alternative approach that allowed assessment of treatment effects while retaining the autocorrelated noise structure. We elected to apply "intervention analysis" (Box *et al.,* 1994), where the "intervention" was emplacement of the treatment. Intervention analysis takes advantage of a time series within which one knows when an intervention occurs but does not know its effect. Backscatter strength at any one time from a pixel, bs_t is modeled as the sum of two components, a treatment effect ω and noise structure or time dependency z_t,

$$bs_t = \omega x_t + z_t. \tag{1}$$

The step function x_t equals zero or unity when t refers to a pre-treatment or treatment scan, respectively. The time dependency determined from the pre-treatment time series is assumed to persist during the treatment scans and be modeled as Box-Jenkins type autoregressive integrated moving average (ARIMA) process (Box *et al.,* 1994), and ω thereby estimates the additional effect of the treatment over the noise.

Noise structure of pre-treatment time series (z_t in Eq. 1) displayed characteristics of a moving-average process. The series were nonstationary, trending up or down, requiring trend removal by differencing. The differenced time series, i.e., change in backscatter, were stationary with zero mean. Only the lag-1 (2.4-h) autocorrelation coefficient (Pearson's r) was significantly greater than zero, and the partial autocorrelation function tended to decrease exponentially, so we fitted a first-difference, moving-average process, IMA [0,1,1] in the notation of Box *et al.* (1994), to the pre-treatment time series, where,

$$z_t - z_{t-1} = a_t - \theta a_{t-1}, \quad -1 < \theta < 1. \tag{2}$$

Thus, the sequential change in backscatter strength $z_t - z_{t-1}$ is the function of a "white-noise" or random time series a_t, where correlation one time step apart (as opposed to time separation of two or more time steps) is determined by the magnitude of θ. The time series a_t represents "random shocks" that drive the system and are the deviations between measured and forecasted values; θ, a dissipation rate, designates how much of the random shock carries over into the process at the next time step.

The noise-structure model specifies a white-noise sequence as input to a "black-box" or transfer function which then generates the data time series as output. Model fitting reverses the process with data as input and white noise (i.e., a random, non-autocorrelated time series) as output. The best that can be expected of a fitted model is non-autocorrelated residuals and minimized squared residuals, achieved with the least number of parameters. To a first approximation, θ and the first-difference, lag-1 autocorrelate ρ_1 are related by (Box *et al.,* 1994)

$$\rho_1 = \frac{-\theta}{1 + \theta^2}. \tag{3}$$

Positive θ's are fitted to the data when ρ_1 is negative. We refined our estimate of θ by least squares. For each pre-treatment time series θ was iterated from −1 to 1 in increments of 0.001. The best-fit value of θ minimized the sum of the squared differences (σ_a^2) between forecast and observed backscatter strength. One-step-ahead forecasts $\hat{bs}_{t+1}$ were predicted as

$$\hat{bs}_{t+1} = (1 - \theta)bs_t + \theta\hat{bs}_t, \tag{4}$$

where bs_t equals the *actual* backscatter strength measured and $\hat{bs}_t$ equals the value *forecast* for time t. The forecast turns out to be an exponentially weighted average of current and past values,

$$\hat{bs}_{t+1} = \lambda bs_t + \lambda\theta bs_{t-1} + \lambda\theta^2 bs_{t-2} + \ldots, \tag{5}$$

where $\lambda = 1 - \theta$ (Box *et al.,* 1994). Values of θ near zero (λ near 1) place greater dependency on values in the near past for a forecast; conversely, large θ and small λ indicate that dependence reaches further back in time. Muth (1960) suggested a useful way of thinking about θ and λ as the proportions of the one-step-ahead random shock that are dissipated and absorbed, respectively, in the ongoing process.

The estimator for the treatment effect $\hat{\omega}$, under the assumptions of an IMA [0,1,1] noise structure model and step change (as opposed to, say, linearly increasing or hyperbolically saturating change) treatment effect is,

$$\hat{\omega} = (1 - \theta)\left(\sum_{s=0}^{p} \theta^s bs_{t+1+s} - \sum_{s=0}^{p} \theta^s bs_{t-s} \right), \tag{6}$$

with nominal variance var $[\hat{\omega}] = \sigma_a^2(1 - \theta^2)$, and turns out to be the difference between weighted averages, one stepped forward in time from the emplacement (first summation), the other stepped backward, the result multiplied by $\lambda = 1 - \theta$ (Box *et al.,* 1994). The only criterion for the number of time steps P is that it be large enough that the last element contributes insignificantly to the summation. We used $P = 40$. Empirical frequency distributions of $\hat{\omega}$ were generated from non-treatment pixels as a further check on the probability levels assigned to the treatment effects.

f. Sediment characteristics

During the experiments, we measured sediment geoacoustic properties *in situ* with pulse techniques that utilize time-of-flight and amplitude measurements between pairs of compressional and shear wave probes (Richardson, 1997a). Divers drove geoacoustic probes into the sediment in a diver-deployed version of an *in situ* sediment acoustic measurement system (ISSAMS; Barbagelata *et al.,* 1991). We measured compressional and shear-wave speeds and attenuation over path lengths ranging from 30 to 60 cm at a depth of 30 cm below the sediment-water interface. For compressional wave measurements, transmit pulses were 38- and 58-kHz pulsed sine waves, and time delays and voltages resulting from the pressure pulses were used to determine values of sound speed and attenuation between identical, radial-poled, ceramic cylinders. We calculated actual values of sound speed and attenuation by comparison of received signals transmitted through the sediment with those transmitted through seawater overlying the sediments. We measured shear speed as time of flight between bimorph bender elements mounted in flexible silicone rubber mounts and driven at 250 Hz.

Scuba divers carefully collected 20 sediment samples, using 6.1-cm inside diameter polycarbonate corers, for physical and geoacoustic properties (14 cores) and for sediment permeability (6 cores). They also collected rectangular slabs of sediment ($30 \times 20 \times 2$ cm in width, depth and thickness, respectively). We measured sediment sound speed and attenuation with an acoustic pulse technique (Richardson, 1986) at 1-cm depth intervals for sediment retained within the cores. Bistatic measurements transmitted and received a 400-kHz sine wave through the sediment and core liner using a pair of identical, fix-mounted, ceramic transducers encased in oil-filled, rubber housings. We used differences in time delays and amplitudes measured in sediment and a distilled-water reference to calculate values of sound speed and attenuation. We corrected all laboratory compressional speeds to *in situ* conditions based on measured pressures, temperatures and salinities.

After we logged the cores acoustically, we extruded and subsampled the sediments at 2-cm intervals for analysis of grain size, grain density, porosity, and wet bulk density. We estimated porosity by weight loss from samples kept in a drying oven at 105°C for 24 h. We measured grain density with a Quantachrome™ Penta-Pycnometer and calculated sediment bulk density from the measured values of grain density and porosity and the calculated value for seawater density. We determined grain-size distributions by dry

sieving for gravel and sand and by Micrometrics SediGraph and pipette for silt and clay particles (Briggs, 1994).

We collected X-radiograph cores from two locations near the ensonified area to document visually the heterogeneity due to sedimentological and biological structures. We X-rayed sediment slabs within a few hours of collection with a Kramex model PX-20N portable X-ray unit. We measured sediment shear strength with a diver-operated torque gauge attached to 21.9 × 21.9-mm vane blades (Briggs and Richardson, 1996) in seven sets of measurements just outside the acoustically scanned area.

We measured bottom roughness photogrammetrically (Briggs, 1989). We collected fourteen stereo pairs along a 15-m transect oriented at 270° (compass bearing) beginning 10 m from the BAMS tower. We digitized a 53-cm transect (at 270°) in each of nine stereo pairs, choosing the segment for clarity and representation of bottom features. We used the resultant roughness profiles to estimate an average roughness power spectrum, and calculated its average slope and intercept (Jackson *et al.,* 1996).

3. Results and discussion

a. Generalizability and success of the manipulations

The overall objective of the manipulations was to test the hypothesis, generated *a posteriori* by Jumars *et al.* (1996) and Briggs and Richardson (1997) from acoustic records with BAMS, that patches of increased animal abundance and activity could be resolved acoustically. Our intent in choosing animals for transplant into the West Sound site was to find species that possibly would have effects representative of major functional groups of organisms, that were not initially present at high abundance and that would have reasonable chance of survival over the few days or weeks remaining in the experiment after manipulations.

We chose *Brisaster latifrons* because it is the same species implicated in 40-kHz backscatter effects by Jumars *et al.* (1996) at 90 m depth off northern California. We have routinely maintained it in the laboratory for other studies for over a year in 15 cm of water in a sea table, and its gonads mature there, so we expect that it survived the manipulation, although we have no information on its susceptibility to ambient predators at Orcas Island. We have similar success maintaining *Molpadia* and observing gonadal maturation when specimens are maintained in darkened outdoor sea tables containing 30 cm of mud in the laboratory at Friday Harbor Laboratories, Friday Harbor, San Juan Island, WA.

We chose bivalves as being very likely candidates to increase backscatter at this mud site. The difficulty was in choosing suitable species for sediment with little mechanical strength in the upper few centimeters. We sought shallow-dwelling species to avoid acoustic attenuation through sediments and because deep-dwelling bivalves often have difficulty re-establishing burrows as adults. *Acila* is often collected, but its natural history is poorly known. Its shell sculpturing and the breadth and fouling patterns of its shell suggest that, unlike many better-known protobranchs, it burrows sluggishly. It is rarely

found below the upper 1 cm, does live in many sediments of comparable rheology and is found in low abundance at the site, so we had confidence that it would both survive and stay at the sediment surface. Individual *Acila* are too small, however, to be resolved by the 40-kHz signals, whose nominal wavelength is 3.7 cm. Cockles live near the sediment-water interface in shallow, sandy habitats. Within mussel reefs at Griffin Bay, San Juan Island, Washington, we do find living expatriates of *Clinocardium* at comparable water depths to the study site, but they show obvious signs of stress in the form of irregular growth marks, deposits of reduced chemicals on their shells, low tissue mass and maximal sizes of only about 3 cm. We emplaced cockles at West Sound with reasonable assurance that they would not burrow very deeply, but little assurance that they would be able to maintain position and survive at the sediment-water interface or avoid predation.

We expected success in transplanting thalassinid shrimp. There is strong evidence from the fossil record that they survive much greater transplant stress in the form of turbidity currents that carry shallow-water species outside their normal depth ranges (Grimm and Follmi, 1994). The caging was essential, as resident *Cancer* assembled rapidly on the outside of the cage, presumably in response to chemical cues, and likely would have eaten uncaged and disoriented specimens. We expected these shrimp to make mounds as they excavated new burrows of about 3 cm diam as they had done in their native site. Artificial burrows and mounds were intended as controls for the thalassinid treatment, and in particular to help tease out the potential contributions to backscatter arising from surficial microtopography versus volume heterogeneity (Jackson and Briggs, 1992).

b. Backscatter strength at 300 kHz

The 300-kHz returns showed range and time dependence (Fig. 3A). Backscatter strength after the Lambert correction tended to increase with range during the study. This "nuisance" trend is reflected in spatial and temporal autocorrelograms of raw data (Fig. 3B, C). Measurements made close together in time or space tended to be similar, i.e., positively (auto)correlated. Rapidly changing average daily backscatter strength during the experimental phase enhanced this artifact in the time domain. Increasing backscatter strength with distance from the tower accounted for the sinusoidal spatial correlogram wherein backscatter strength from adjacent and distant (at the outer edge of the ensonified area) pixels are similar. Backscatter strength from pixels at intermediate inter-pixel distances tended to be dissimilar from that at the edges. Detrending effectively removed most of the spatial autocovariance (Fig. 3B, D).

Diver controls (Fig. 4, 5) revealed a few scattered pixels with time-integrated probability levels around 0.01 that could represent artifacts of the SCUBA diver's disturbance of the bottom during simulated emplacement of a manipulation. Lower combined probabilities among many pixels would indicate that the acoustic properties of the seafloor have changed due to this control manipulation, but such more general changes were not observed.

The *Acila* treatment had the most obvious effect (Fig. 4). All three replicates showed a

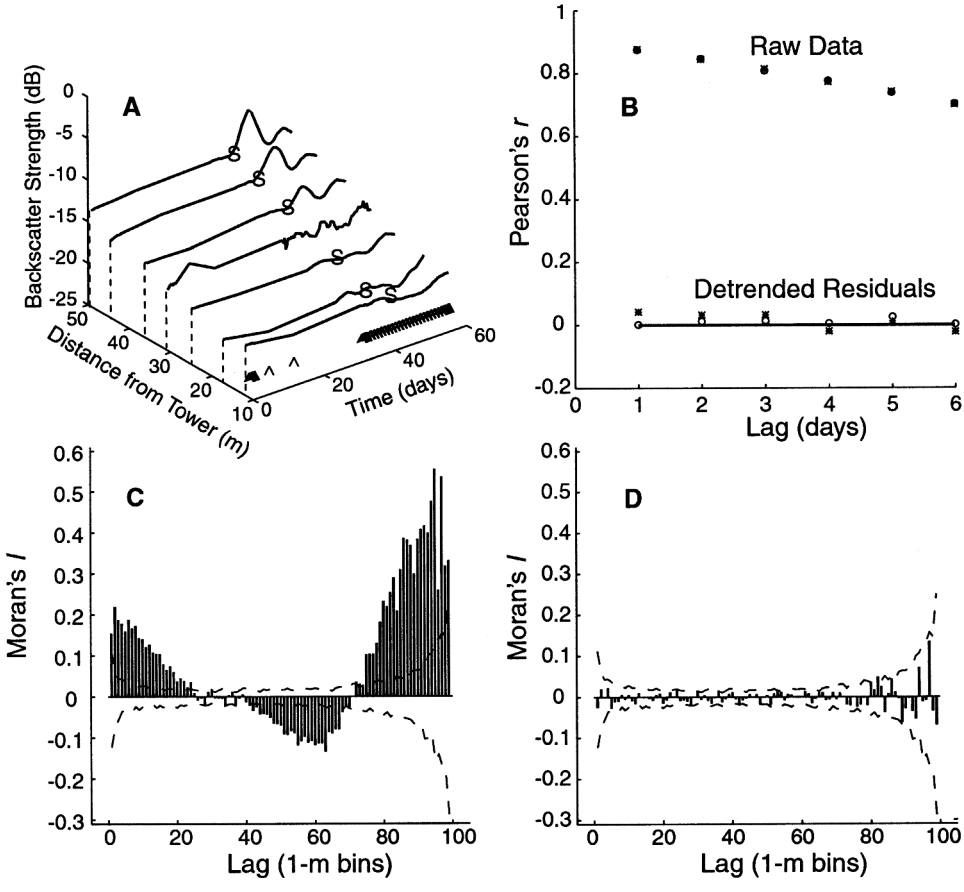

Figure 3. Range and time dependence of 300-kHz backscatter. (A) Azimuthally averaged backscatter strength during the deployment: Carat (^) marks times when scans were made; S = first emplacement (start) of a treatment. At range 31 m the squiggly line shows the usual scan-to-scan variability of average backscatter strength, whereas the other curves are LOWESS smoothings (Cleveland, 1979). (B) Monte Carlo estimation of Pearson's product-moment correlation coefficient at one-day lags based on 22 scans taken at 2200 (O) and 0200 hours (*) from 100 randomly selected pixels before and after accounting for temporal trends. Monte Carlo estimation of Moran's I spatial autocorrelation coefficient based on 1000 randomly selected pixels from 62 scans before (C) and after (D) accounting for spatial trends. Dashed lines are approximate 95% confidence limits for the I coefficient based on 100 repeated estimates of the I coefficients using random normal deviates having the same mean and variance as the original data.

compact, contiguous area of significantly increased backscatter strength ($P \leq 10^{-5}$) including, or adjacent to, the location of the acoustic marker. These areas were 23, 28 and 45 pixels or 0.8, 0.9 and 1.1 m^2 in area, respectively. Generally, backscatter strength in the *Acila* treatment remained constant for the duration of the experiment. Of the 96 pixels examined near the marker locations after treatment, only 6 had sample Kendall's τ

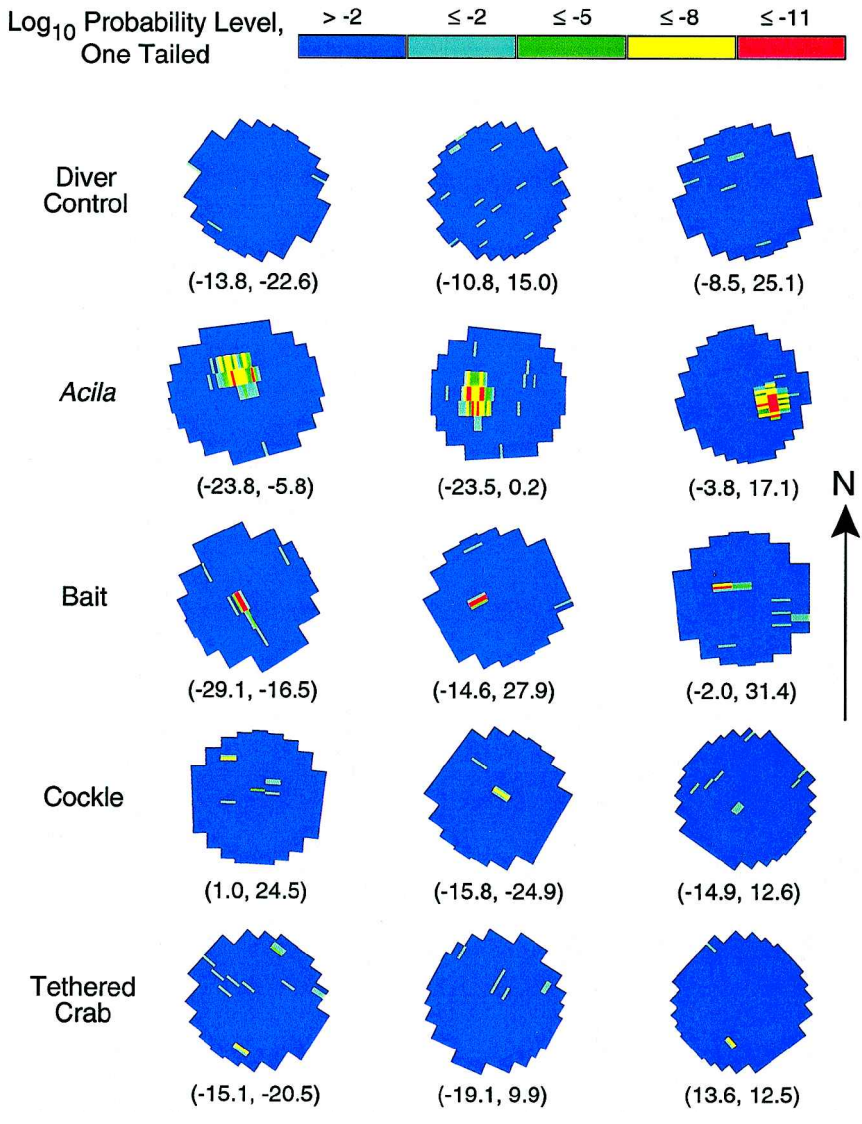

Figure 4. Plan view of treatment effects at 300 kHz with color-scaled combined probability levels for each treatment replicate. Pixels are 1° in azimuthal and 0.075 m in radial extent. For these treatments, the null hypothesis of no significant change in backscatter intensity was tested one tailed against the anticipated increase. The rough "circle" comprises 221–521 pixels (each of 7.5 cm radial and 31–75 cm azimuthal extent) within the 12.5-m^2 search zone. Coordinates are in the two-dimensional Cartesian reference frame shown on the axes of Figure 2, with origin at the tripod.

correlation coefficients in the 5% tail of an empirical distribution of τ from untreated pixels ($\tau_{emp} = 0.0 \pm 0.32$, mean $\pm$ 2 SD, $n = 3400$ untreated pixels). The overall effect was to increase backscatter strength by about 9 $\pm$ 18 dB (Table 1). Increased backscatter strength

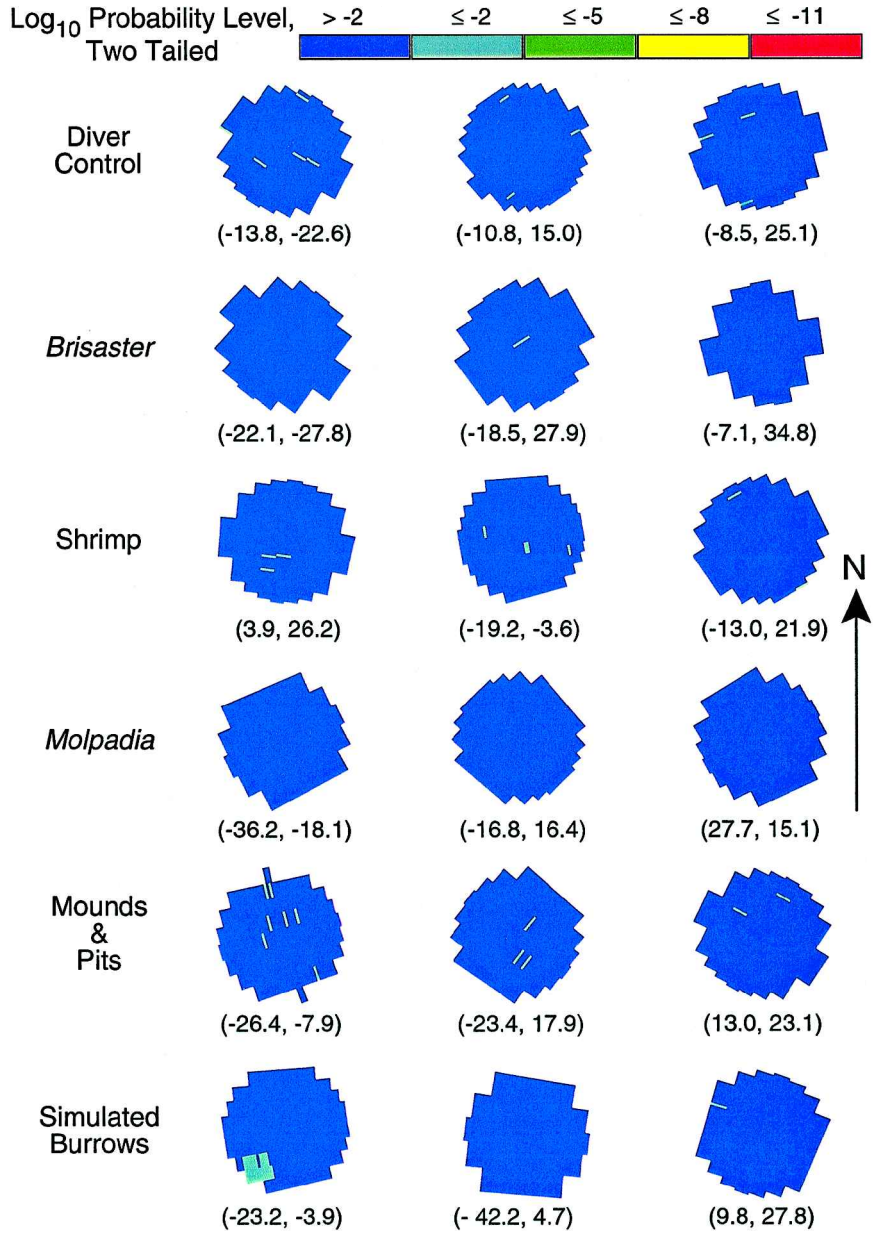

Figure 5. Plan view of treatment effects at 300 kHz with color-scaled combined probability levels for each treatment replicate. Pixels are 1° in azimuthal and 0.075 m in radial extent. For these treatments, the null hypothesis of no significant change in backscatter intensity was tested two tailed because the direction of change was not predicted *a priori*. The rough "circle" comprises 221–521 pixels (each of 7.5 cm radial and 31–75 cm azimuthal extent) within the 12.5-m^2 search zone. Coordinates are in the two-dimensional Cartesian reference frame shown on the axes of Figure 2, with origin at the tripod.

Table 1. Summary of significant treatment replicates (300-kHz) from those pixels with combined probabilities $\leq 10^{-5}$ in Figures 4 and 5.

Treatment	X (meters) East positive from Tower	Y (meters) North positive from Tower	Pre-treatment N (scans) [days]	Treatment N (scans) [days]	Number of Pixels with combined $P \leq 10^{-5}$ [total in area]	"before" Mean pre-treatment backscatter strength ± 2SD (dB)	"after" Mean treatment backscatter strength ± 2SD (dB)
Acila	−23.8	−5.8			23 [383]	−1.3 ± 9.0	7.1 ± 9.5
Acila	−23.5	0.2	34 [44]	26 [11]	28 [399]	−0.7 ± 8.3	7.8 ± 8.9
Acila	−3.8	17.1			45 [521]	−0.2 ± 8.8	9.3 ± 9.5
Bait	−29.1	−16.5			4 [283]	−1.2 ± 5.4	16.2 ± 16.9
Bait	−14.6	27.9	30 [42]	30 [13]	3 [301]	−2.9 ± 14.2	15.0 ± 5.2
Bait	−2.0	31.4			3 [299]	−0.1 ± 12.9	10.7 ± 2.0
Cockle	−15.8	−24.9			1 [309]	−1.4 ± 8.0	6.7 ± 9.4
Cockle	1.0	24.5	32 [43]	28 [12]	2 [387]	0.8 ± 6.7	7.0 ± 9.1

is not surprising, as the shells (1.0 cm) are almost exactly 2 wavelengths (1500 m s^{-1}/ 300,000 s^{-1}) in diameter, and very high areal densities were used. Because we have samples and X-radiographs of *Acila castrensis* in life position at the sediment-water interface in West Sound, it is the only one of the manipulations in which we have reasonable confidence that animals stayed near the sediment-water interface.

Two of the cockle replicates showed single, isolated, but centrally located (i.e., the expected location of the treatment) pixels with significantly increased backscatter strength (Fig. 4). One of these two also had a significant pixel near the outer edge of the 2-m search area. The third cockle replicate resembled the diver controls (coordinates −14.9, 12.6). From examining the time series, it is apparent that backscatter strength from one cockle replicate abruptly increased then decreased over time while the other monotonically increased (Fig. 6A, B). Two mechanisms might explain this time and site dependence. Depth of burrowing may differ between replicates and change over time, placing some individuals below the depth of effective sound penetration. Another possibility is differential mortality in a suboptimal mud habitat from attraction of predators or scavengers to feed on the cockles. In addition to changing scattering from the cockles, such predators and scavengers themselves are likely to scatter sound. Potential organisms include brittle stars, sea stars, crabs, rays and other fishes. Since it is not clear why the time dependence differs between sites and only a small number of pixels is involved, we compared "before" and "after" averages (Table 1). The increase was about 7 ± 17 dB.

Bait treatments also significantly increased backscatter strength (Fig. 4; 6C, D). Each replicate had 4–6 contiguous significant pixels, with significance level decreasing away from the center. One replicate (coordinates −2.0, 31.4) also had a cluster of significant pixels in one corner caused by the placement of a large object (part of another experiment) 4 d before the end of our data collection. Curiously, in two replicates the bait-induced increase decayed with time, while in the third, it grew larger (Fig. 6C, D). Backscatter from the rebar and cat food container alone does not explain the temporal change. Declining backscatter strength is consistent with attractants washing out of the can over time and

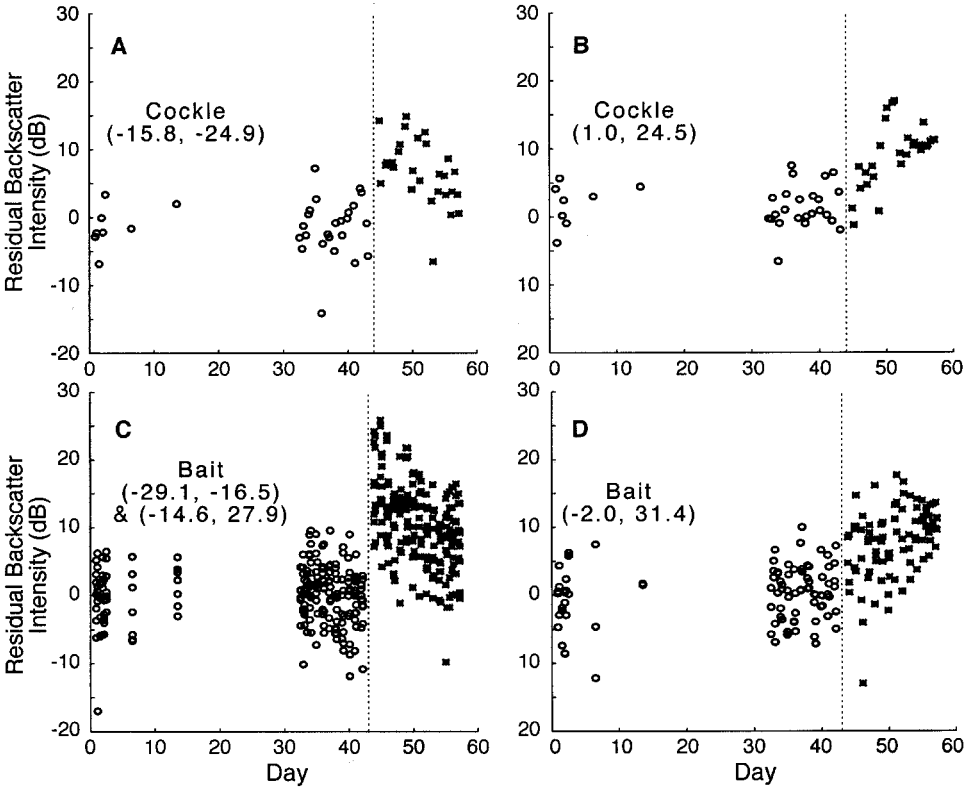

Figure 6. Time series of 300-kHz backscatter strength for the cockle (top) and bait treatments. Vertical line indicates time of placement of 10 cockles or the bait. (A) Values from a single pixel within the search area of a cockle replicate showing an abrupt increase upon placement, followed by linear decay (Kendall's $\tau = -0.37$, $P = 0.006$, $n = 28$). (B) Values from a single pixel within the search area of a cockle replicate in which backscatter strength increased linearly with time (Kendall's $\tau = 0.46$, $P = 0.001$, $n = 28$). The second centrally located high-backscatter pixel within the search area did not show a statistically significant change over time (Kendall's $\tau = -0.15$, $P = 0.19$, $n = 28$). (C) Pixels from two replicates combined showing an abrupt increase after placement of the bait, followed by linear decay (Kendall's $\tau = -0.28$, $P = 0.04$, N = 210). (D) The third bait replicate in which backscatter strength increased linearly with time (Kendall's $\tau = 0.26$, $P = 0.05$, $n = 90$). Probability levels for τ were deduced from an empirical distribution of 3400 untreated pixels.

leading to dispersal of the formerly attracted scavengers. The replicate in which backscatter strength increased was near the introduced object noted above. Perhaps the placement of more objects nearby served as an attractant (e.g., by sediment resuspension), or perhaps bait in this can was slowest to wash out, leading to aggregation of individuals from previous treatments. SCUBA divers often found crabs huddled against the acoustic marker, suggesting thigmotaxis or a general response to disturbance (e.g., to chemical signals of sediment resuspension) and structure on an otherwise featureless bottom.

We expected only a few pixels at or close to the bait to be affected over the post-treatment period. Many single strong acoustic reflectors such as fishes or crabs, likely to be attracted to a plume emanating from the can, would need to be in those pixels for each of the 30 post-treatment scans over 13 d to register a higher-than-expected backscatter strength relative to all the pre-treatment scans. To determine the magnitude of increase in backscatter strength for the bait treatment if backscatter decreased with time we averaged over affected pixels for the night before the acoustic marker was put down and compared to averaged values for the night after the marker was removed. If backscatter strength increased with time we averaged values for the night before the acoustic marker was put down and the last scan. Although the variance is high, backscatter strength increased by about 15 ± 19 dB (Table 1).

Two of the tethered-crab replicates showed isolated pixels with high backscatter strength along the edge of the 2-m search area and the third resembled the diver control (Fig. 4). The off-center location is consistent with placement of the T-handled reinforcing bar away from the acoustic marker so that the crab's tether would not tangle with the float line attached to the marker. In the replicate not showing any pixels with high backscatter strength, the short ½-in (1.3 cm) width of the T handle may have been facing the tower, while in the other two replicates the 5-in (13 cm) length faced the tower. Subsequent analysis within a search area centered on the presumed rebar did not show any additional pixels with high backscatter strength. Our conclusion is that the pixels with significant increase in backscatter strength are due to echoes off the rebar. If an individual crab is detectable at 300 kHz, then single instances of high backscatter, occurring in many pixels, a likely description of a tethered crab moving about, would be difficult to resolve from background noise.

We are especially puzzled by the lack of a treatment effect for urchins (Fig. 5). Urchin tests are large enough to backscatter 300-kHz energy, and the urchin treatments were resolved in associated side-scan surveys (D. Van Holliday, BAE SYSTEMS, personal communication). Side scans were conducted at 100 and 500 kHz on the day of the urchin deployment. One hint from some of the scans is that bright reflectors (the presumed urchins) showed up at the ends of less bright "trails," suggesting that the urchins may have dispersed relatively rapidly from the treatment pixels, i.e., failed to stay within a 2-m range of the target sphere.

Pixels with many scans in either or both tails of backscatter strength would have been detected by the two-tailed analysis (Fig. 5). All treatments analyzed two tailed resembled the two-tailed diver controls. A patch of significantly different pixels in one of the simulated burrow replicates is due to unintended overlap with an *Acila* replicate.

c. Backscatter strength at 40 kHz

The 40-kHz backscatter data consisted of 585 scans at 2.5-h intervals for each of 317 treatment pixels with approximate average dimensions 0.5 × 2 m (Fig. 2B). Spatial autocorrelation did not uncover any systematic patchiness (correlograms not shown)

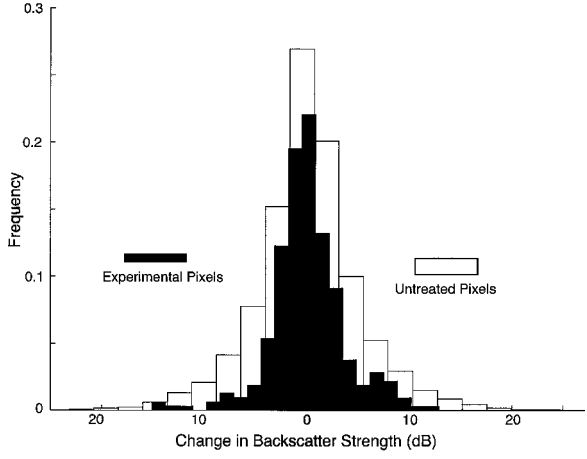

Figure 7. Comparison of frequency distributions of change in 40-kHz backscatter strength ($\hat{\omega}$ in Eq. 6) for experimental (solid, $n = 317$ pixels) and untreated ($n = 963$ pixels $\times$ 7 trials = 6174) pixels. $\hat{\omega}_{untreated} = 0.10 \pm 5.1$ and $\hat{\omega}_{experimental} = 0.15 \pm 3.6$ (mean $\pm$ SD).

within the ensonified area. Nor was periodicity at diurnal or tidal frequency evident. Time series from all treatment pixels (and perhaps all pixels in the ensonified area) shared characteristics indicative of a nonstationary, first-order, moving-average process (IMA [0,1,1] sensu Box *et al.,* 1994): Only the lag-1 autocorrelation coefficient was significantly less than zero, and exponential decay dominated the partial autocorrelation function. First differencing (i.e., conversion to between-scan change in backscatter strength) was required to transform the nonstationary series into a stationary one.

For us the "interventions" in intervention analysis (Box *et al.,* 1994) were emplacement of animal and bio-mimic treatments. Pre-treatment time series varied in length but were about 400 scans long, an ample number for fitting an IMA model. Acoustic markers were in place for about 10 scans, leaving approximately 175 treatment scans. Under the null hypothesis, the expected change in backscatter strength ($\hat{\omega}$ in Eq. 1) is zero. The magnitude of $\hat{\omega}$ is determined by the difference between the forward-stepped weighted average and backward-stepped weighted average. The weighting is θ^s, where s is the time step and θ ranges from -1 to 1. Thus backscatter measurements just after and just before emplacement carry the greatest weight. No consistent pattern of treatment effects emerged from the analysis (Fig. 7). Only 6 of 317 treatment pixels had values of $\hat{\omega}$ that deviated >2 SD from the mean. One was from a diver control, suggesting that the other five may also have been artifacts of diver actions.

We did not find convincing treatment effects at 40 kHz. To be of interest, negative results generally require analysis of statistical power. Further, the realization that many future remote-sensing experiments will comprise time series (perhaps at 300 kHz or higher frequencies that did detect some of our treatments) prompted us to survey properties of the

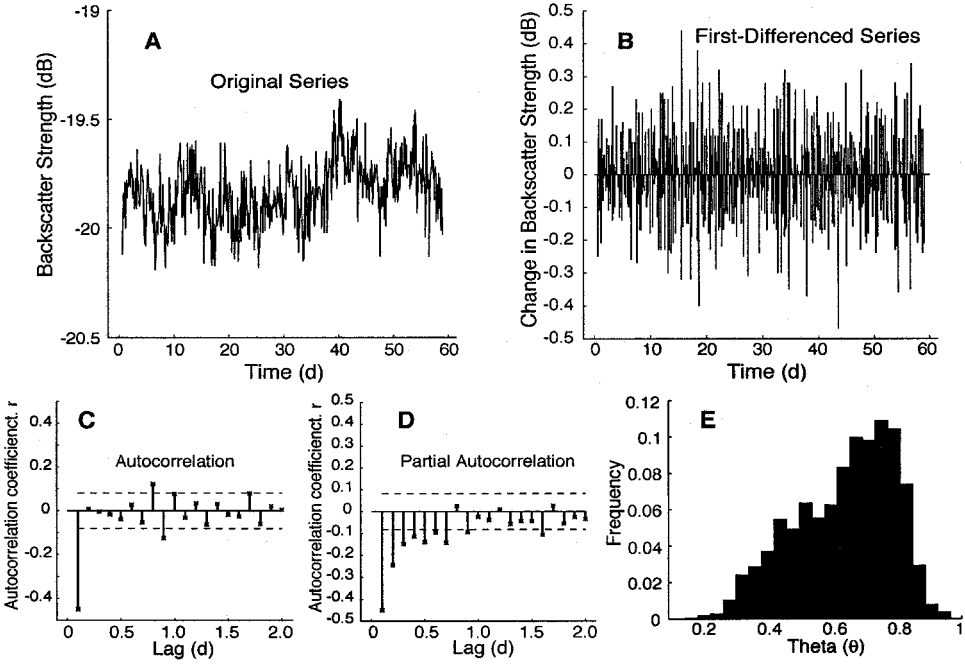

Figure 8. (A) Time series of 40-kHz average backscatter strength (dB) from the 963 untreated pixels of Figure 2B. (B) First differencing of series A (i.e., change in backscatter strength) removes nonstationarity, giving a stable mean around zero. (C) Autocorrelation and (D) partial autocorrelation functions of the first-differenced series show characteristic behavior of an IMA [0,1,1] model. Dashed lines are ±2 standard errors. (E) Frequency distribution of θ (Eq. 4) fitted to the untreated pixels.

time series that may prove useful for characterizing benthic environments. We used the empirical stochastic properties of untreated pixels to estimate the minimum detectable change in backscatter strength for this environment, then examined its use for detecting outlier events.

Of the 40-kHz pixels, 963 lacked experimental manipulations (Fig. 2B). Taking the average backscatter strength across these pixels at each time point, we formed a single time series embodying the stochastic characteristics of the area (Fig. 8A). First differencing gave a stationary series with fixed mean around zero (Fig. 8B). Behaviors of the autocorrelation and partial autocorrelation functions (Fig. 8C, D) are characteristic of a first-order, moving-average process (Box *et al.,* 1994). The lag-1 (2.4-h) autocorrelation coefficient is significantly different from zero and much larger in absolute value than coefficients at larger lags. Further, the partial autocorrelation function decreases exponentially to values that could be accounted for by sampling error. The frequency distribution of least-squares estimates of the IMA [0,1,1] model parameter (θ in Eq. 4) indicates a modal value of approximately 0.75 (Fig. 8E).

Substituting 0.75 for θ in Eq. 2–6 gives a simple relationship for making one-step-ahead forecasts of backscatter which would be characteristic of this environment and time of year $\hat{bs}_{t+1} = 0.25bs_t + 0.75\hat{bs}_t$. The forecast is computed using information already in hand: the value of the previous forecast $\hat{bs}_t$ and the current measured backscatter strength bs_t. All historical information is contained in these coefficients that summarize past environmental changes capable of altering backscatter strength. For example, a change in seawater temperature between scans, which affects sound speed in water versus sediment and therefore potentially the backscatter strength, may contribute to the difference in backscatter strength between successive scans. Also contributing are pelagic and benthic point sources of scatter. If any single source had been prominent on time scales of, say, 0.5 or 1 d, we would expect the autocorrelation function to reflect this periodicity. There is a suggestion of diurnal periodicity at lags 8 and 9, but they are neither consistent (one positive and the other negative) nor as prominent as the correlation at lag 1 (Fig. 8C).

To illustrate outlier detection, we fitted an IMA [0,1,1] model to the noise structure of the first 100 scans of a selected pixel (Fig. 9). The least-squares fit parameter (θ) is 0.75 and standard deviation (SD) of the residuals is ±3.5 dB. For simplicity we assume that this model also applies to the next 485 scans, but we could have re-assessed it at any number of scan intervals. The ±2 SD detection threshold is approximately ±7 dB. In this case we have explicitly defined "unusual" as being any future backscatter strength that deviates from the one-step-ahead model forecast by ±7 dB, placing the deviation outside the 95% confidence interval of the first 100 residual backscatter strengths. By contrast, the ±2 SD range in the raw data distribution about the simple mean of the first 100 scans is ±10 dB; 43% broader than significant deviations from the time-series model. The overall signal-to-noise ratio hasn't changed. Gain in sensitivity comes from using otherwise wasted information contained in immediate past noise levels to make a more accurate and precise one-step-ahead forecast. The forecast series (Fig. 9B) captures the general trend of the original series, and the residuals (Fig. 9C) indicate that the model is adequate. Placement and removal of the acoustic markers are clearly distinguishable from background noise in the deviate series (Fig. 9D), more so than in the nonstationary and highly variable original series.

ARIMA-type models capture the interaction between the highly stochastic marine benthic environment and deterministic physics of acoustics. Thus this approach holds promise for future acoustic manipulations and also is likely to be useful for other long ecological time series with few replicates in space, i.e., for the usual situation in environmental monitoring. Remote surveillance of benthic environments with sonar has many more challenges compared with aerial surveillance with radar. There is the obvious clutter of reflectors ranging over a few orders of magnitude in size in marine environments compared to a relatively empty sky. Sizes and concentrations of these reflectors vary in time and that time variation is reflected in the echo time series, making it difficult to pick out deviations from the norm except perhaps by a trained observer viewing the whole series (e.g., Fig. 9A). Simultaneous viewing of many data series from many pixels from a

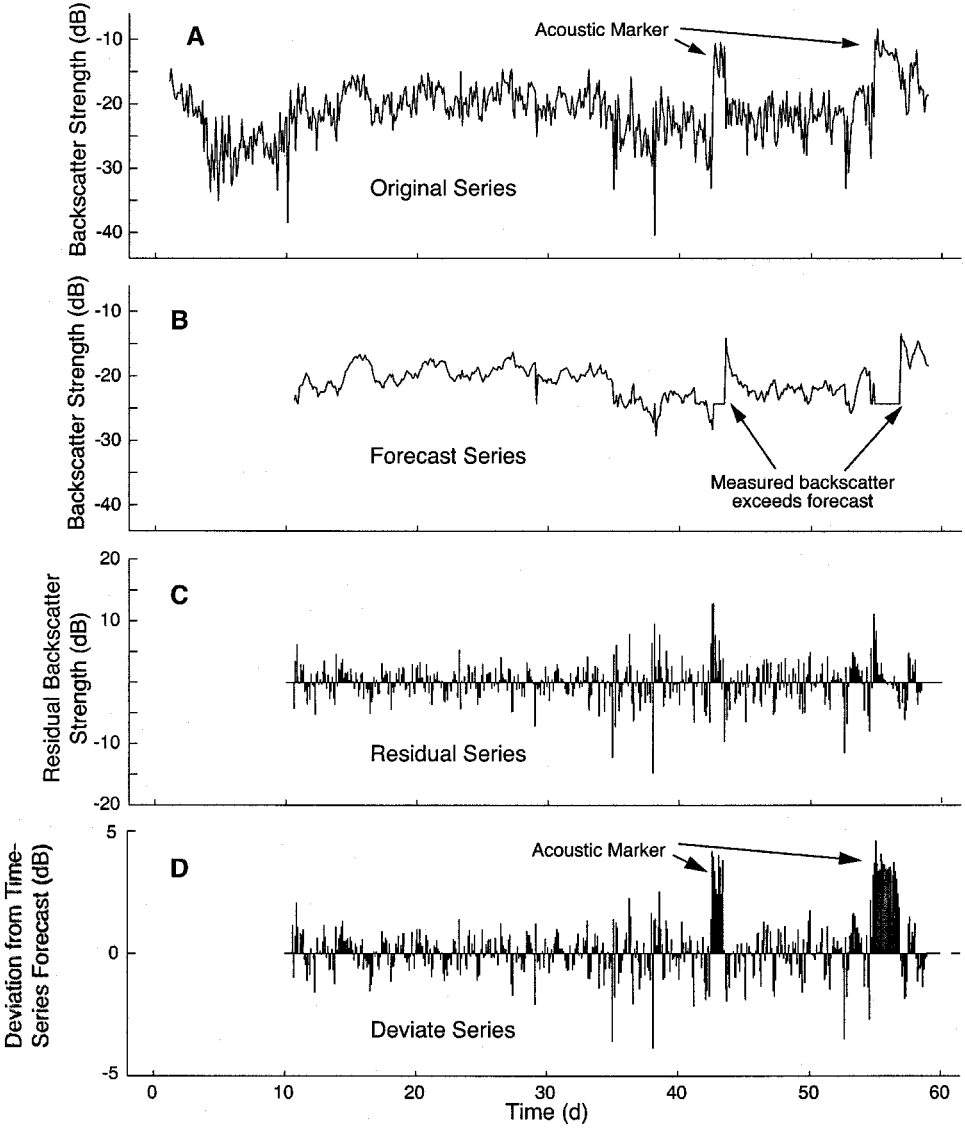

Figure 9. Original (A), forecast (B), residual (C) and deviate (D) time series showing detection of two markers with sustained backscatter strengths exceeding 7 dB above forecasts. (A) Measured time series. The first 100 scans (10 d) were used to fit an IMA [0,1,1] model. The result: $\hat{bs}_{t+1} = 0.25bs_t + 0.75\hat{bs}_t$, SD = 3.5 dB. On detecting a deviation [((original − forecast)/SD)) ≥ 2], the forecast reverts to the series-average backscatter strength of −24.3 dB. (C) The residual series (original − forecast) does not show a coherent pattern, indicating model adequacy, except when outliers are detected. (D) The first marker was retrieved after 10 scans. The second marker remained until the last scan, at which point backscatter strength had diminished slightly. Presence of each marker is clearly distinguishable from background noise.

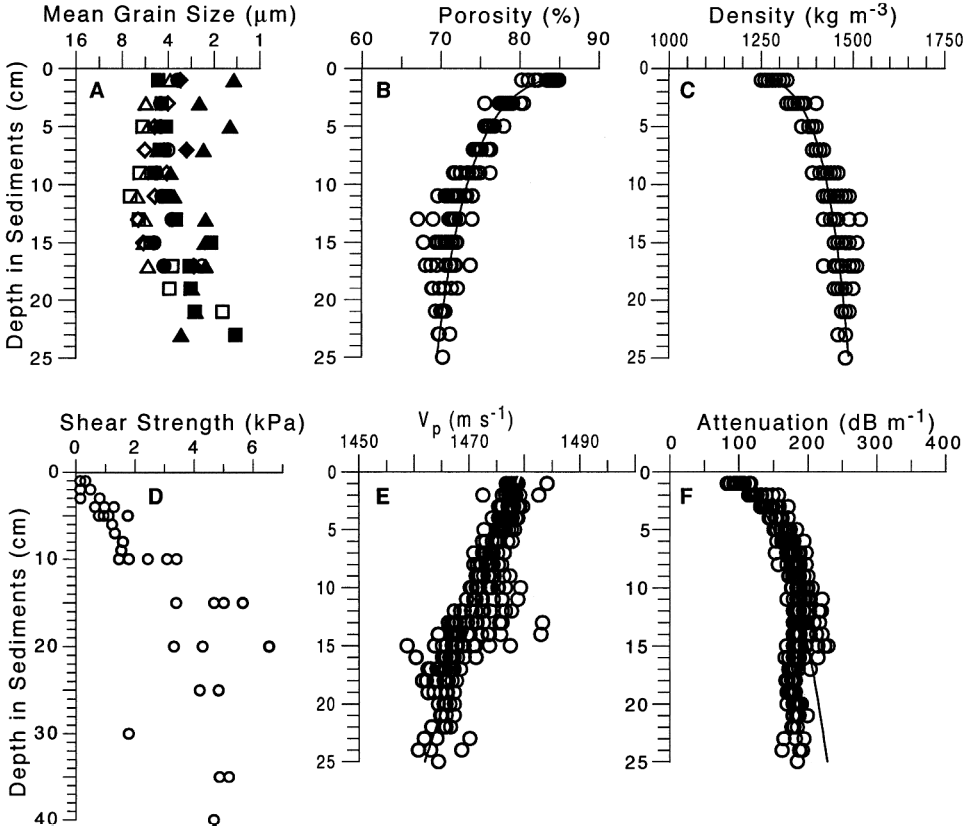

Figure 10. Geoacoustic properties of West Sound mud. Grain size (A), porosity (B) and bulk density (C) were measured from core samples but shear strength (D) was measured *in situ.* Sound speed (E) and attenuation (F) versus depth were measured at 400 kHz in diver-collected cores.

large area is impractical. Radar-like color-coded computer screen representations of ARIMA model determinations of deviations (e.g., Fig. 4, 5) from ambient fluctuations permit accurate surveillance of large areas. Resetting the threshold level used alters sensitivity. A 4-SD level would exclude all but the largest deviations. Pixels with chronically high or low deviate values are easily weeded out for more detailed attention.

d. Sedimentary structure and acoustic properties

A natural question, which can be addressed based on the measured geoacoustic parameters, is whether any of our treatments at 40 kHz should have shown backscatter in excess of 7 dB above or below natural time-varying fluctuations and therefore should have been detectable. Sediments were predominantly very poorly sorted, clayey silts with $< 2\%$ sand. Mean grain size ranged between 1.4 and 6.8 μm with no apparent depth gradient (Fig. 10A). Mollusk shells, found in only 10% of the 2-cm deep subsamples of cores, were

also evident in X-radiographs. Most of the shell material was in live specimens of *Acila castrensis.* Average sediment porosity was 74.1%, with a marked reduction with depth over the upper 12 cm (Fig. 10B). The depth distribution of sediment bulk density was the mirror image of porosity, and values varied from 1280 kg m^{-3} near the surface to 1470 kg m^{-3} below 12 cm (Fig. 10C).

Fine-scale variation of sediment bulk density was evident in X-radiographs of sediment cores collected from the experimental site. Sediments in the upper 7–10 cm appeared well mixed by recent bioturbation. Burrows and other feeding traces that are common in other muddy sediments were rare. Below 10 cm were remnants of layered deposits, partially disrupted by bioturbation, followed by stiffer, more consolidated sediment. A sharp increase in sediment shear strength at 10 cm corroborates this interpretation (Fig. 10D).

Values of *in situ* sound speed in surficial sediments (1457 m s^{-1} at 38 kHz; 1462 m s^{-1} at 58 kHz) were 1.9–2.2% *lower* than the speed in the overlying seawater (1490 m s^{-1}). Values of attenuation were both variable and quite low (averaging 2.7 dB m^{-1} at 38 kHz and 5.7 dB m^{-1} at 58 kHz). Because sound speed in surficial sediments was lower than in seawater, there was no critical angle and sound refracted into the sediment at all grazing angles. It thus could reflect back from shells or other volume heterogeneities. Shear wave speed (mean 25 m s^{-1}), a measure of sediment rigidity, was also low. In summary, the range and variability of values of sediment geoacoustic properties measured in sediments near and within the Orcas acoustic experimental site are characteristic of highly bioturbated, surficial muddy sediments (Richardson, 1997b).

Values of sound speed and attenuation measured at 400 kHz from the diver-collected cores were significantly higher than sound speed and attenuation measured *in situ* at 38 and 58 kHz. The higher laboratory-measured sound speed can be accounted for based on the gradient in sound speed with depth in these muddy sediments (Fig. 10E). Values of laboratory-measured sound speed converged with the *in situ* sound speed (near 1460 m s^{-1}) at depths of 30 cm. The negative gradient in sound speed with depth was a result of the dominance of changes in bulk density compared to compressibility in these very low-porosity sediments. In contrast to the situation involving compressional wave velocity, gradients in compressional wave attenuation do not explain the obviously higher values of laboratory attenuation compared to *in situ* values. For the frequency range considered here, the increase in intrinsic attenuation with frequency should be approximately linear. In other words, an attenuation value of 2.7 dB m^{-1} at 38 kHz is equivalent to 4.2 dB m^{-1} at 58 kHz and 28.6 dB m^{-1} at 400 kHz. Values of laboratory attenuation (400 kHz) were near 175 dB m^{-1} at sediment depths greater than 10 cm (Fig. 10F). Sediment disturbances due to coring or other artifacts are too small to account for the differences (Richardson, 1997b). The presence of layers and other forms of spatial heterogeneity may result in acoustic scattering at the higher laboratory frequencies and dominate signal loss in the laboratory measurements.

The sediment-water interface was practically featureless in the stereo pairs. Average RMS roughness was 0.40 cm; slope (−3.2) and intercept (5.2×10^{-5} cm^3) of the

Table 2. Roughness model inputs for compared sites. Bottom-water sound speed $V_w = 1490$ m s^{-1}.

Site	f (kHz)	V_R	$\sigma^2_{V_p}$ (m^2 s^{-2})	k (dB m^{-1} kHz^{-1})	l_ρ (cm)	ρ_R	$\sigma^2_\rho \times 10^{-3}$	μ	$\delta \times 10^{-3}$	γ_1 (cm^4)	$\omega_1 \times 10^{-5}$ (cm^3)
Orcas	40	0.98	25.1	0.07	2.7	1.4	4.0	−0.85	1.9	3.23	5.2
	300	0.99	25.1	0.43	2.7	1.4	4.0	−0.85	11.7	3.23	5.2
Diga	40	0.97	14.9	0.06	10.2	1.5	5.5	−0.89	1.6	—	—
	300	0.97	14.9	0.09	10.2	1.5	5.5	−0.89	2.4	—	—
Eel River	40	1.02	802.4	0.11	2.0	1.8	7.0	−1.8	3.1	—	—
	300	1.02	802.4	0.53	2.0	1.8	7.0	−1.8	14.8	—	—

roughness power spectrum indicated a dearth of high-frequency spatial roughness at the time of sampling. The lack of high-frequency roughness suggests very little recent modification of the sediment-water interface by biological processes or more likely a mechanical inability of surficial sediments to hold shape.

For the purposes of acoustic modeling, a sound-speed gradient ($V_p = 1479 - 0.7z$), where z is depth in centimeters, adequately accounted for sound-speed distribution. Porosity (%) decreased with depth ($=80.1z^{-0.008}$) whereas bulk density (g cm^{-3}) increased ($=1.28z^{0.05}$). (Although it is given as a continuous function, the porosity expression was derived from data of 1-cm resolution and is ill behaved for $z < 1$). These gradients probably resulted from a combination of dewatering deeper sediments through compaction by burrowing infauna and fluffing the sediments through the activities of other animals near the surface. It is doubtful that bioturbation by the resident benthic fauna or physical processes related to storms would result in values of sound speed, porosity or bulk density significantly outside these ranges.

e. Modeling of acoustic backscatter

To help understand the paucity of significant experimental results, we modeled acoustic backscattering using parameters derived from the diver cores, in-situ measurements and seafloor stereo photography following Jackson *et al.* (1996). Relevant sediment parameters (Table 2) are bottom-water sound speed (V_w), sound speed (V_R) ratio between sediment and water (V_p/V_w), sound-speed variance in sediments ($\sigma^2_{V_p}$), sound-speed attenuation (k), density correlation length (l_ρ), density ratio (ρ_R) of sediments to water (ρ/ρ_w), density variance (σ^2_ρ), ratio of compressibility to density fluctuations (μ), loss parameter (δ), 1-dimensional roughness spectral slope ($-\gamma_1$), and 1-dimensional roughness spectral intercept (ω_1). Due to nonlinear frequency dispersion within the sediment, two sets of average values of geoacoustic inputs in Table 2 are given, one for the *in situ* 38-kHz measurements matching the frequency of the backscatter measurements at 40 kHz, and the other set for the laboratory 400-kHz measurements approximating the frequency of the backscatter measurements at 300 kHz. The statistical inputs characterizing fluctuations of sediment sound speed are derived from diver core measurements.

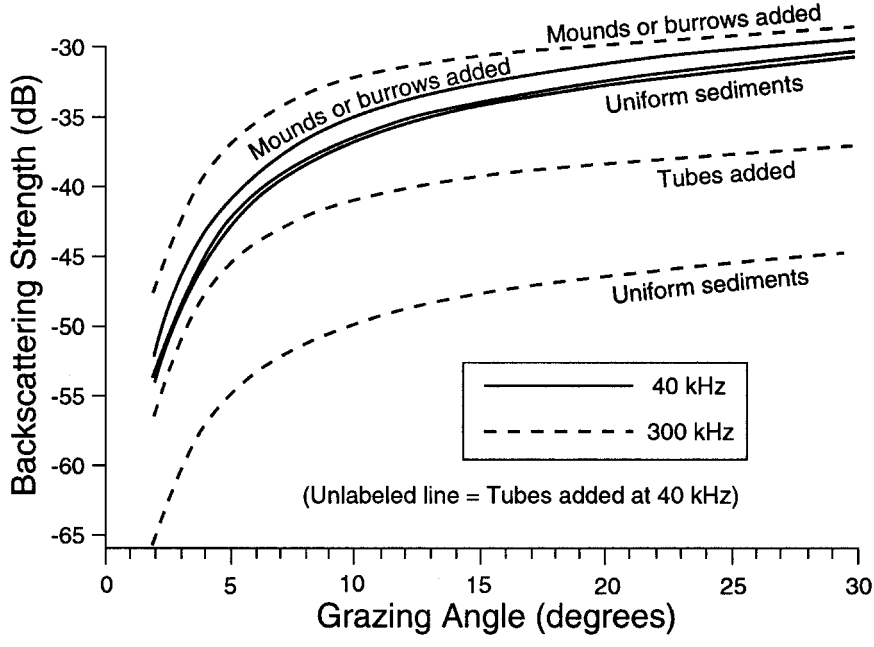

Figure 11. Backscatter predicted at 40 and 300 kHz from West Sound sediments. Predictions use the parameter values of Table 2 and the composite backscatter model of Jackson *et al.* (1996).

From the Orcas parameters in Table 2, a composite roughness model (Jackson *et al.,* 1996) predicts very low levels of acoustic backscattering strength (<-31 dB) for either 40 or 300 kHz. Predictions for 40 kHz are 12 to 14 dB greater than for 300 kHz within the range of grazing angles used (Fig. 11). Of the two components of backscattering, sediment volume scattering dominates over interfacial roughness scattering, especially at 40 kHz. These predictions are determined largely by the lack of impedance contrast between the water and sediment as well as the lack of interfacial roughness.

In order to gauge the effects of changes in interfacial roughness and sediment physical and geoacoustic properties we can manipulate the model parameters within reasonable ranges and observe the changes in acoustic response. The seafloor microtopography is the most featureless within our experience among about a dozen sites. If the seafloor were colonized by a low-diversity community of deposit-feeding polychaetes, which increase the high spatial frequency roughness with their tube building, the roughness power spectrum slope and intercept might resemble those estimated for the seafloor in Eckernförde Bay: -2.4 and 30.3×10^{-5} cm^3, respectively (Jackson *et al.,* 1996). At another site deposit feeders cause large roughness features such as mounds and burrows, which increase high- and mid-range spatial frequency roughness, resulting in a roughness power spectrum slope and intercept like those estimated for the seafloor in the Dry Tortugas, FL: -2.3 and 209×10^{-5} cm^3, respectively (Jackson *et al.,* 1996). These two cases represent-

ing increasing effects of bioturbation on interfacial roughness were used together with the Orcas geoacoustic and physical property parameters in Table 2 to generate new predictions of backscattering strength (Fig. 11).

Interfacial roughness at these scales makes a larger difference in predicted backscatter strength for 300 than for 40 kHz. Differences between predictions at 40 kHz for a mound-burrow interface and a tubicolous interface are only 1–2 dB, whereas predictions at 300 kHz for the two roughness types differ by about 9 dB over the 10–20° range of grazing angles consistent with treatment locations (Fig. 2). It is unfortunate, then, that we did not have storage capacity to record enough 300-kHz data for a formal intervention analysis. The acoustic calculations suggest that our "mound-and-pit" treatment would have been detectable in a 300-kHz intervention analysis. Backscattering strength, however, is predicted to be never more than −28.5 dB.

Muds in general do not exhibit much variability in values of measured sound speed or density (Briggs and Percival, 1997). Thus, only small ranges of values for the geoacoustic and physical parameters are credible for substitution in the model. Sound-speed ratio varies from 0.97 to 1.02 in silty clays and clayey silts (Richardson, 1997b). Data on sediment sound speed, sound attenuation, and density from a silty clay at Diga, La Spezia, Italy, and from a clayey silt at station S60 off the Eel River, California, were combined with measured input parameters for water sound speed, roughness spectral slope and intercept at the Orcas experiment site to generate additional predictions (Fig. 12).

As indicated by greater values of sound speed variance ($\sigma^2_{V_\rho}$) and density variance (σ^2_ρ), sediments measured from the Eel River site have much greater variability than sediments from the Diga site (Table 2). This greater variability is almost certainly due to the intense bioturbation occurring at the Eel River S60 site, transitional nature of its sediment type (mixed sands and muds), and presence of storm layers. Furthermore, the high correlation length characteristic of density at the Diga site is indicative of a homogeneous sediment versus the greater heterogeneity—shorter correlation length in sediment density—at the Eel River site. The variability exhibited in the Eel River sediment parameters is responsible for the largest predicted increase in backscattering strength in Fig. 12: 5–9 dB at 40 kHz and 13–17 dB at 300 kHz. Such a large predicted difference between the Orcas and the Eel River analogues is undoubtedly due to the fact that Eel River sediment has a critical angle, whereas the Orcas sediment does not. Thus beyond the critical angle at Eel River microtopography or volume heterogeneity can generate strong backscatter where none would otherwise be expected. We therefore predict that sonar time-series measurements will be most informative about infaunal abundances and activities in sediments that do have a critical angle.

4. Conclusions

In hindsight, with acoustic characterization of the sediments in hand, the rarity of significant experimental effects at the Orcas site and their limitation to "hard scatterers" could have been anticipated. Low sound-speed contrast between sediments and bottom

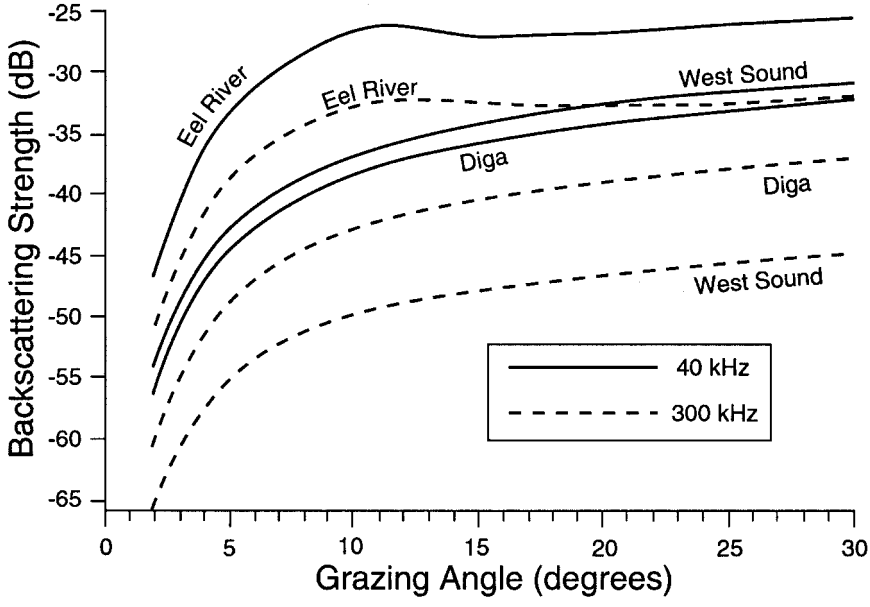

Figure 12. Backscatter expected from sediments of higher sound-speed contrast, namely those found at Diga, La Spezia, Italy (Richardson, 1997b), and the S60 site at Eel River, California (Richardson, 1997b; Richardson and Briggs, 1993). Predictions use the parameter values of Table 2 and the composite backscatter model of Jackson *et al.* (1996).

water and in particular the lower sound speed in surficial sediments than in overlying water or deeper sediments gives little opportunity for backscatter by simulated burrows, natural burrows of thalassinid shrimp, mounds and pits or other surficial topography. Conversely, greater biogenic influence on backscatter via modification of microtopography and via variation in sound speed (volume heterogeneity) can be expected in sediments with greater sound-speed contrast from seawater. It is clear that the presence of sediments and site-to-site variations in sedimentary characteristics make acoustic assessment of benthos fundamentally more difficult than assessment of plankton and nekton. This disadvantage in ability to detect organisms themselves is offset, however, by the potential to detect organism activities recorded in the sedimentary medium in the acoustically resolvable form of time variations in volume heterogeneity and microtopography. Despite the failure of most of our treatments to generate significant acoustic effects, our study demonstrates that for one site and some infaunal and demersal taxa and abundance patterns, acoustics can give unprecedented spatial and temporal resolution.

Acknowledgments. This study was supported by the U.S. Office of Naval Research. We thank A.O.D. Willows, the Director of Friday Harbor Laboratories, for generous access to the animal maintenance and boat facilities needed to carry it out. Christopher D. Jones, D. Van Holliday and Kevin L. Williams provided stimulating discussions. Two anonymous reviewers helped us to improve the final presentation.

REFERENCES

Barbagelata, A., M. D. Richardson, B. Miaschi, E. Muzi, P. Guerrini, L. Troiano and T. Akal. 1991. ISSAMS: An *in situ* sediment geoacoustic measurement system, *in* Shear Waves in Marine Sediments, J. M. Hovem, M. D. Richardson, and R. D. Stoll, eds., Kluwer Academic Publishers, Dordrecht, The Netherlands, 612 pp.

Box, G. E. P., G. M. Jenkins and G. C. Reinsell. 1994. Time Series Analysis: Forecasting and Control, Prentice-Hall, Englewood Cliffs, NJ, 598 pp.

Briggs, K. B. 1989. Microtopographical roughness of shallow-water continental shelves. IEEE J. Ocean. Eng., *14,* 360–367.

——— 1994. High-frequency acoustic scattering from sediment interface roughness and volume inhomogeneities. Ph.D. Dissertation, Univ. Miami, Coral Gables, FL, 143 pp.

Briggs, K. B. and D. B. Percival. 1997. Vertical porosity and velocity fluctuations in shallow-water surficial sediments and their use in modeling volume scattering, *in* High Frequency Acoustics in Shallow Water, N. G. Pace, E. Pouliquen, O. Bergem and A. P. Lyons, eds., NATO SACLANT Undersea Res. Ctr., La Spezia, Italy, 612 pp.

Briggs, K. B. and M. D. Richardson. 1996. Variability in *in-situ* shear strength of gassy muds. Geo-Mar. Lett., *16,* 189–195.

——— 1997. Small-scale fluctuations in acoustic and physical properties in surficial carbonate sediments and their relationship to bioturbation. Geo-Mar. Lett., *17,* 306–315.

Cleveland, W. S. 1979. Robust locally weighted regression and smoothing scatterplots. J. Am. Stat. Assoc., *74,* 829–836.

Cliff, A. D. and J. K. Ord. 1973. Spatial Autocorrelation, Pion Press, London, 178 pp.

Dworski, J. G. and D. R. Jackson. 1994. Spatial and temporal variation of acoustic backscatter in the STRESS experiment. Cont. Shelf Res., *14,* 1221–1237.

Grimm, K. A. and K. F. Follmi. 1994. Doomed Pioneers: Allochthonous crustacean tracemakers in anaerobic basinal strata, Oligo-Miocene San Gregorio Formation, Baja California Sur, Mexico. Palaios, *9,* 313–334.

Jackson, D. R. and K. B. Briggs. 1992. High-frequency bottom backscattering: roughness vs. sediment volume scattering. J. Acoust. Soc. Amer., *92,* 962–977.

Jackson, D. R., K. B. Briggs, K. L. Williams and M. D. Richardson. 1996. Tests of models for high-frequency sea-floor backscatter. IEEE J. Ocean. Eng., *21,* 458–470.

Jumars, P. A., D. R. Jackson, T. F. Gross and C. Sherwood. 1996. Acoustic remote sensing of benthic activity: a statistical approach. Limnol. Oceanogr., *41,* 1220–1241.

Muth, J. F. 1960. Optimal properties of exponentially weighted forecasts. J. Am. Stat. Assoc., *55,* 299–306.

Nichols, F. H. 1975. Dynamics and energetics of three deposit-feeding benthic invertebrate populations in Puget Sound, Washington. Ecol. Monogr., *45,* 57–82.

Press, W. H., B. P. Flannery, S. A. Teukolsky and W. T. Vetterling. 1988. Numerical Recipes in C. Cambridge University Press, NY, 735 pp.

Richardson, M. D. 1986. Spatial variability of surficial shallow water geoacoustic properties, *in* Ocean Seismo-Acoustics, T. Akal and J. M. Berkson, eds., Plenum Press, NY, 527–536.

——— 1997a. Attenuation of shear waves in near-surface sediments, *in* High Frequency Acoustics in Shallow Water, N. G. Pace, E. Pouliquen, O. Bergem and A. P. Lyons, eds., NATO SACLANT Undersea Res. Ctr., La Spezia, Italy, 612 pp.

——— 1997b. *In-situ,* shallow-water sediment geoacoustic properties, *in* Shallow-Water Acoustics, R. Zhang and J. Zhou, eds., China Ocean Press, Beijing, China, 163–170.

Richardson, M. D. and K. B. Briggs. 1993. On the use of acoustic impedance values to determine sediment properties. Proc. Inst. Acoust., Vol. 15, Pt. 2, Acoustic Classification and Mapping of the Seabed, 15–24.

Skolnik, M. I. 1980. Introduction to Radar Systems, McGraw-Hill, NY, 581 pp.
Sokal, R. R. and F. J. Rohlf. 1995. Biometry, W. H. Freeman, San Francisco, CA, 887 pp.
Urick, R. J. 1983. Principles of Underwater Sound, McGraw-Hill, NY, 423 pp.
Williams, K. L. 2001. Temporal fluctuations in the acoustic scattering from bottom-deployed objects and localized biological treatments. IEEE J. Ocean. Eng., *26,* 63–69.

Received: *19 June, 2001;* revised: *18 September, 2001.*